Supporting Information

Exposed High-Concentration Ir Active Sites and Metal–Support Interaction Endow Ir/MoO_2-Mo_2C Hybrids with High Atom Utilization and Stability for pH-Universal Hydrogen Evolution Reaction

Yuehuan Zhang and Qiang Yuan*

State Key Laboratory of Green Pesticide, Center for R&D of Fine Chemicals, College of Chemistry and Chemical Engineering, Guizhou University, Guiyang, Guizhou province 550025, PR China.

E-mail addresses: qyuan@gzu.edu.cn

Experimental section

Chemicals

Iridium chloride ($IrCl_3 \cdot xH_2O$; reagent grade) was purchased from Aldrich. Ammonium molybdate tetrahydrate ($(NH_4)_6Mo_7O_{24} \cdot 4H_2O$; 99%) was purchased from Macklin. Dopamine hydrochloride (98%) was purchased from Aladdin. Melamine (99%) was purchased from J&K Chemical. Boric acid (99%) was purchased from Aladdin. Ammonia solution (AR) was purchased from Chuandong Chemical. Moreover, 20% Pt/C and 10% Ir/C were purchased from Premetek Co. and Aladdin, respectively. IrO_2 was purchased from Alfa Aesar. All reagents and chemicals were used as received without any further purification.

Synthesis of hollow Mo_2C

Mo_2C was synthesized by following previously reported methods.[1] First, 370 mg ammonium molybdate tetrahydrate was dissolved in 30 mL ultrapure water, followed by the addition of 200 mg dopamine hydrochloride under stirring for 20 min. Subsequently, 60 mL ethanol solution was added and stirred for 5 min before pouring 0.5 mL ammonia solution, under continuous stirring for 3 h. The obtained Mo-PDA composite was centrifugally washed with ethanol and dried. Subsequently, it was heated to 800 °C at a rate of 5 °C/min under Ar atmosphere and held for 2 h. The tube furnace-treated sample was etched with sulfuric acid, centrifugally washed with ethanol, dried, and finally yielded the hollow molybdenum carbide support.

Synthesis of Ir/MoO_2-Mo_2C-800

First, 20 mg hollow Mo_2C powder, 20 mg boric acid, and 30 mg melamine were dispersed in 40 mL ultrapure water and stirred for 10 min. Thereafter, 500 μL of a 0.05 mol/L $IrCl_3$ solution was added, followed by continuous stirring for 12 h. The resulting mixture was oven-dried at 80 °C for 5 h. The

obtained powder was heated to 800 °C at a rate of 5 °C/min and held for 2 h. Finally, the reacted powder was etched with sulfuric acid, washed and centrifuged with ethanol, and stored in 5 mL ethanol solution. Similarly, Ir/MoO_2-Mo_2C-600 and Ir/MoO_2-Mo_2C-700 were synthesized using the same method, except for the pyrolysis temperatures (600 °C and 700 °C, respectively).

Material characterizations

The surface morphology and elemental composition of the catalyst were characterized using transmission electron microscopy (TEM; JEM-1400 Flash, 120 kV) and double spherical aberration-corrected high-angle annular dark-field scanning transmission electron microscopy (HAADF-STEM; FEI Spectra 300). The elemental composition was analyzed by inductively coupled plasma optical emission spectroscopy (ICP-OES) (Thermo Fisher Scientific, iCAP 7200). The crystal structure of the catalyst was determined by X-ray powder diffraction (XRD; Bruker D8 Discover). The chemical valence state and surface atomic ratio were collected by X-ray photoelectron spectroscopy (XPS, ESCALAB 250Xi). The extended X-ray absorption fine structure (EXAFS) was measured at Taiwan Photon Source (TPS) beamline, 44A Quick-scanning X-ray absorption spectroscopy (XAS), in National Synchrotron Radiation Research Center (NSRRC), Hsinchu, Taiwan. In situ Raman measurements were performed using a LabRAM HR Evolution spectrometer with 532 nm excitation wavelength. The measurements of in-situ attenuated total reflection surface-enhanced infrared absorption spectroscopy (ATR-SEIRAS) were performed on a Nicolet-iS50 FT-IR spectrometer equipped with a liquid nitrogen-cooled MCT-A detector.

XAFS data processing

The XAFS data were processed following standard procedures using the Athena module in the IFEFFIT software package. The EXAFS spectra were obtained by subtracting the postedge

background from the total absorption and subsequently normalizing them relative to the edge jump step. The $\chi(k)$ data were Fourier-transformed into real (R) space using a Hanning window (dk = 1.0 $Å^{-1}$) to isolate the EXAFS contributions from different coordination shells. Least-squares curve fitting was performed using the ARTEMIS module in the IFEFFIT software package to obtain quantitative structural parameters around the central atom. [2, 3]

Electrochemical measurements

The electrochemical activity of the prepared catalysts was measured using a standard three-electrode system (CHI 760E). The working electrode was a glassy carbon electrode coated with the catalyst, the counter electrode was a graphite rod, and the reference electrode was Hg/HgO in alkaline conditions or Ag/AgCl in acidic/neutral conditions. All polarization curves were recorded in 0.5 M H_2SO_4, 1.0 M KOH, and 1.0 M PBS solutions, respectively. The catalyst ink was prepared by mixing 5 mg of the catalyst with 500 μL ethanol and 500 μL of 0.1% Nafion solution, followed by ultrasonication for 30 min to obtain a homogeneous catalyst ink. The catalyst ink was uniformly drop-cast onto the surface of a glassy carbon (GC) electrode (5 mm diameter) with an Ir loading of 5.05 μg cm^{-2}. For commercial Pt/C and Ir/C, the metal loading on the GC electrode was 10.2 μg cm^{-2}. The measured potentials were converted to the reversible hydrogen electrode (RHE) scale using the following equations:

$E_{vs\ RHE} = E_{Ag/AgCl} + 0.197 + 0.059pH$ in 0.5 M H_2SO_4 or 1.0 M PBS

$E_{vs\ RHE} = E_{Hg/HgO} + 0.098 + 0.059pH$ in 1.0 M KOH

The polarization curves of all samples were recorded in N_2-saturated electrolyte at a rotation rate of 1600 rpm and a scan rate of 10 mV s^{-1} by applying IR compensation applied. Electrochemical impedance spectroscopy (EIS) measurements were conducted in the frequency range of 0.01-100 kHz

with an AC amplitude of 5 mV. The electrochemical active surface area (ECSA) of the samples was determined by measuring the double-layer capacitance (C_{dl}) through cyclic voltammetry (CV) tests at scan rates ranging from 20 to 120 mV s^{-1} within the non-Faradaic potential window. The long-term stability was evaluated via continuous cyclic voltammetry (CV) in the potential range of -0.1 to 0.1 V (vs. RHE) at a scan rate of 100 mV s^{-1}.

The HER kinetics of the catalyst were evaluated from the Tafel slopes, obtained by analyzing the polarization curves using the Tafel equation ($\eta = b \log(j) + a$).

Mass activity (MA) reflects the intrinsic activity of the prepared noble metal catalyst and was calculated as follows:[4]

$$j_{mass\ activity} = \frac{j_{geo} \times A_{geo}}{m_{Ir}}$$

where m_{Ir} represents the mass of Ir loaded on the GC electrode as determined by ICP-OES analysis, A_{geo} denotes the geometric area, and j_{geo} denotes the geometric current density.

The turnover frequency (TOF) is calculated using the following formula:[5]

$$TOF = \frac{\text{Total Hydrogen Turn Overs Per Geometric area}}{\text{Active Sites Per Geometric area}}$$

The total number of hydrogen turnover

$$= \left(|j|\ \text{mA cm}^{-2}\right)\left(\frac{1\ \text{C s}^{-1}}{1000\ \text{mA}}\right)\left(\frac{1\ \text{mol e}^{-}}{96485.3\ \text{C}}\right)\left(\frac{1\ \text{mol}}{2\ \text{mol e}^{-}}\right)\left(\frac{6.022 \times 10^{23}\ \text{molecules H}_2}{1\ \text{mol H}_2}\right)$$

$$= 3.12 \times 10^{15} |j| \frac{H_2\ (s^{-1})}{cm^2}\ \text{per}\ \frac{mA}{cm^2}$$

The number of active sites in Ir/MoO_2-Mo_2C-800 was calculated based on the total mass of Ir at the electrode, assuming each Ir atom occupies one catalytic active site.

Actives Sites =

$$\frac{\text{mass loading} \times \text{catalyst loading per geometric area} \left(\frac{\text{g}}{\text{cm}^2}\right)}{\text{Ir } M_W \left(\frac{\text{g}}{\text{mol}}\right)} \left(\frac{6.022 \times 10^{23} \text{ Ir atoms}}{1 \text{ mol Ir}}\right)$$

$$= 1.59 \times 10^{16} \text{ Ir active sites/cm}^2$$

Finally, the current density from the polarization curve can be converted to TOF values using the following equation.

$$\text{TOF} = \frac{3.12 \times 10^{15}}{1.59 \times 10^{16}} \times |j|$$

The ATR-SEIRAS measurements were conducted in a custom-designed three-electrode cell, which consisted of a gold film working electrode, an Ag/AgCl reference electrode, and a platinum foil counter electrode. The chronoamperometric measurements were performed in both alkaline and acidic electrolytes, with voltage scan ranges of 0 to -0.35 V and 0 to -0.15 V (vs. RHE), respectively. Infrared spectra were collected at a spectral resolution of 8 cm^{-1}.

Electrochemical measurements in the AEM water electrolyzer

The anion exchange membrane (AEM) water electrolyzer was assembled using carbon paper loaded with Ir/MoO_2-Mo_2C-800 (0.5 mg_{Ir} cm^{-2}) or Pt/C (0.5 mg_{Pt} cm^{-2}) as the cathode, and nickel foam loaded with IrO_2 (2 mg cm^{-2}) as the anode. The electrode active area was 0.25 cm^2. The FAA-3-50 anion exchange membrane was pretreated in 1.0 M KOH at 60 °C for 12 h. The AEM water electrolyzer was operated in 1.0 M KOH electrolyte at 25 °C with a flow rate of 5 mL min^{-1}. The stability of the AEM water electrolyzer was evaluated by chronopotentiometry at 0.2 and 1 A cm^{-2}.

In situ Raman measurement

Measurements were taken using a LabRAM HR Evolution Raman spectrometer equipped with a 532 nm laser. For in situ Raman experiments, a platinum wire was the counter electrode and an

Ag/AgCl electrode was the reference electrode, conducted in 1.0 M KOH and 0.5 M H_2SO_4, respectively. The dynamic evolution of interfacial water during the HER process on Ir/MoO_2-Mo_2C-800 was investigated by acquiring the Raman spectra under different applied potentials using chronoamperometry. The potential in Raman measurements is reported vs Ag/AgCl.

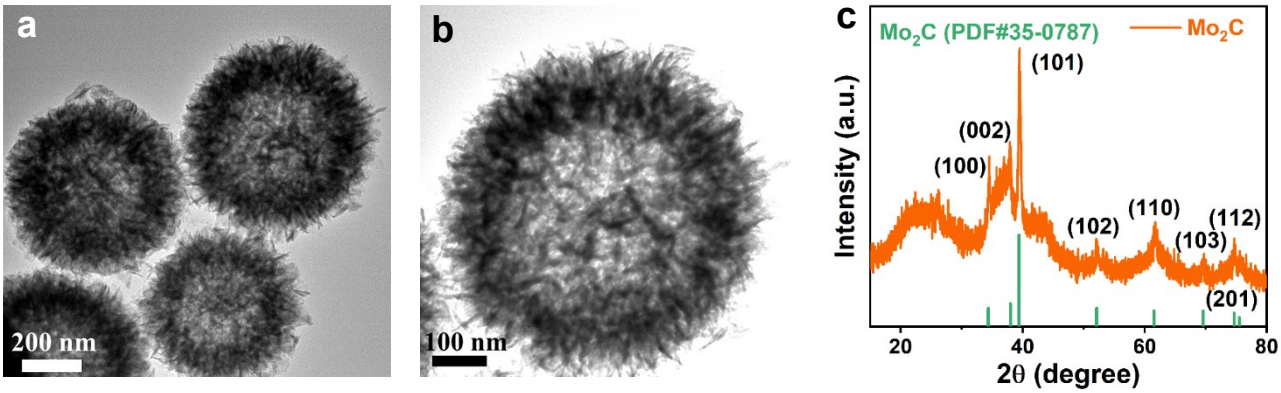

Fig. S1 (a, b) TEM images, (c) XRD pattern of Mo_2C.

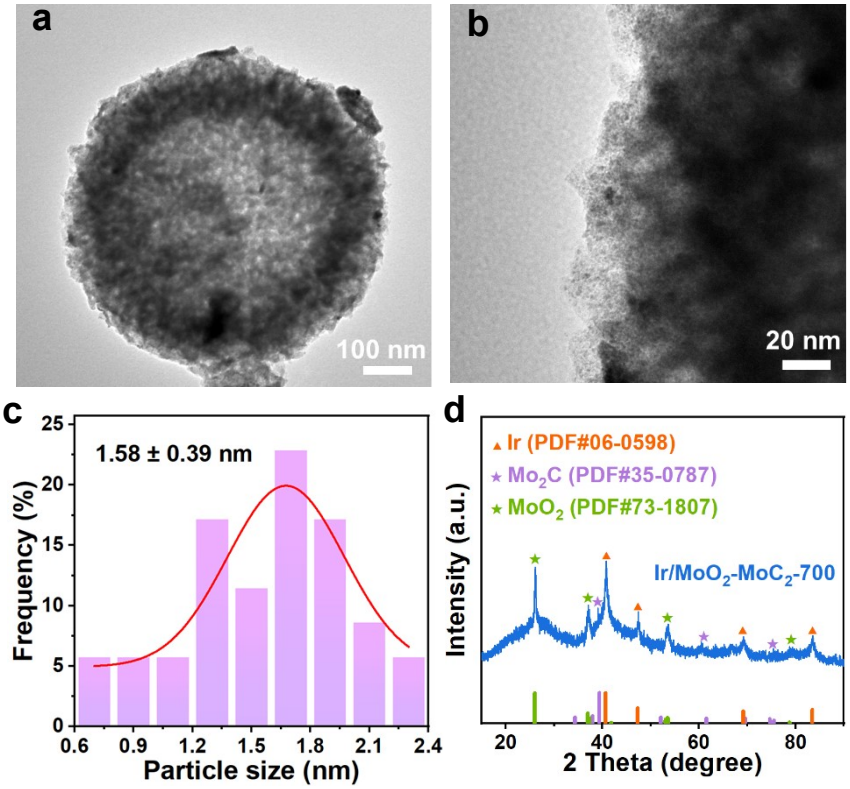

Fig. S2 (a, b) TEM images, (c) the column chart size, and (d) XRD pattern of Ir/MoO_2-Mo_2C-700.

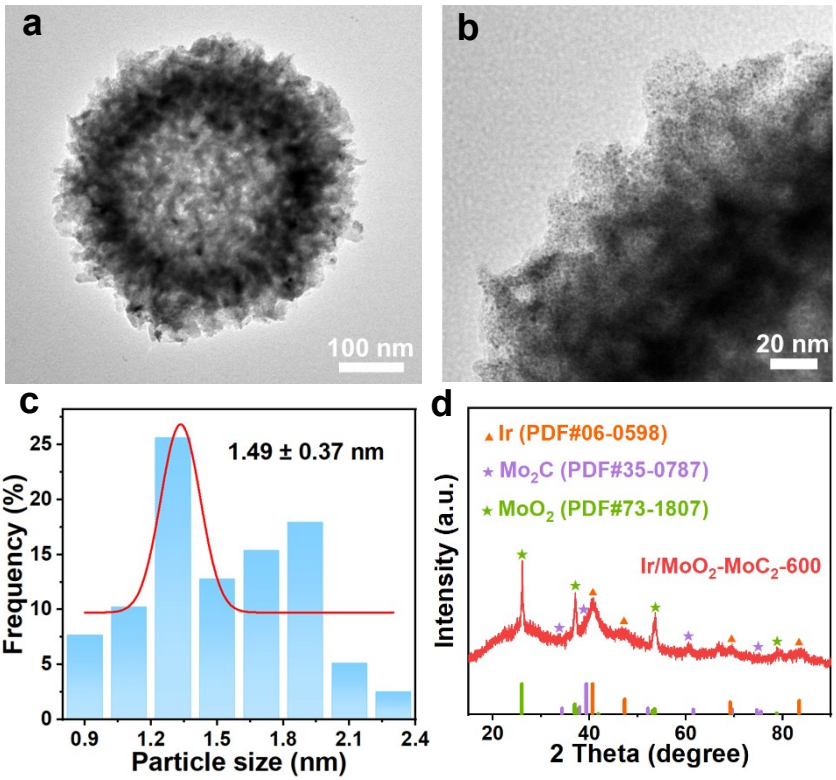

Fig. S3 (a, b) TEM images, (c) the column chart size, and (d) XRD pattern of Ir/MoO_2-Mo_2C-600.

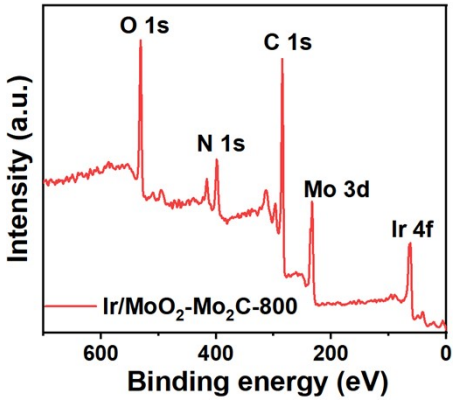

Fig. S4 XPS full spectra for Ir/MoO_2-Mo_2C-800.

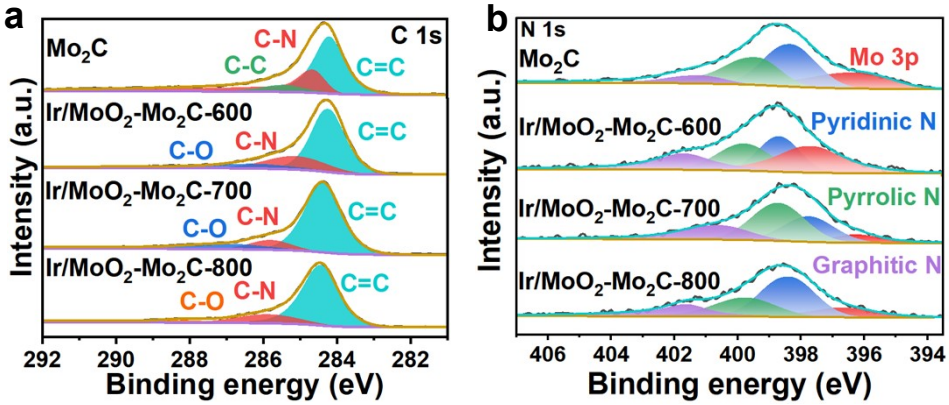

Fig. S5 (a) C 1s and (b) N 1s in Mo_2C, Ir/MoO_2-Mo_2C-600, Ir/MoO_2-Mo_2C-700, and Ir/MoO_2-Mo_2C-800.

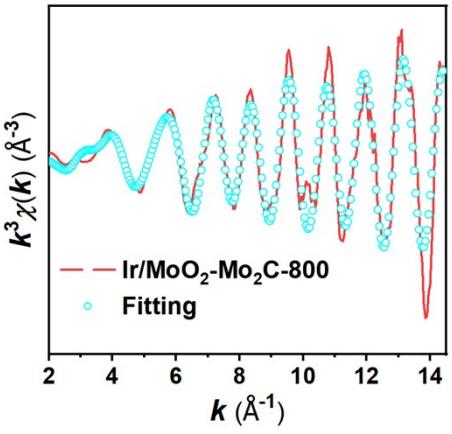

Fig. S6 EXAFS fitting curves of Ir/MoO_2-Mo_2C-800 in the k space.

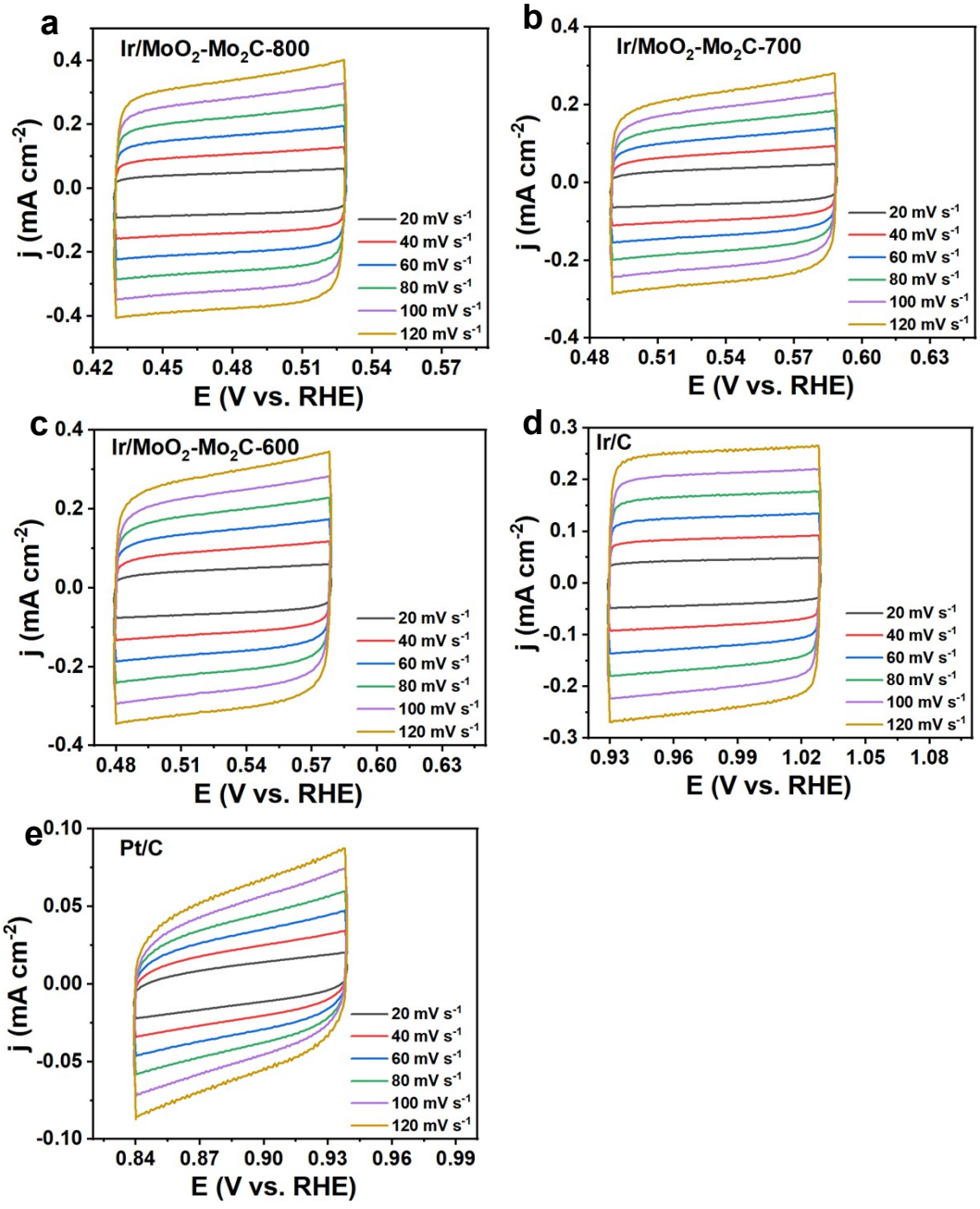

Fig. S7 CV curves of the (a) Ir/MoO_2-Mo_2C-800, (b) Ir/MoO_2-Mo_2C-700, (c) Ir/MoO_2-Mo_2C-600, (d) Pt/C and (e) Ir/C at different scan rates in 1.0 M KOH solution.

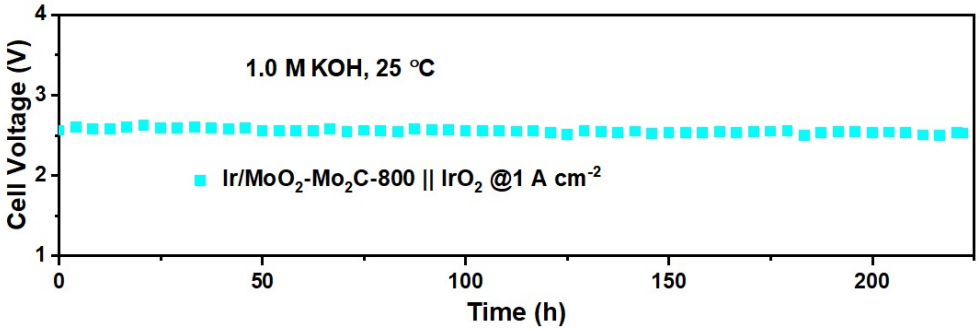

Fig. S8 Chronopotentiometry curve of the AEMWE using Ir/MoO_2-Mo_2C-800 and IrO_2 operating at 1 A cm^{-2}.

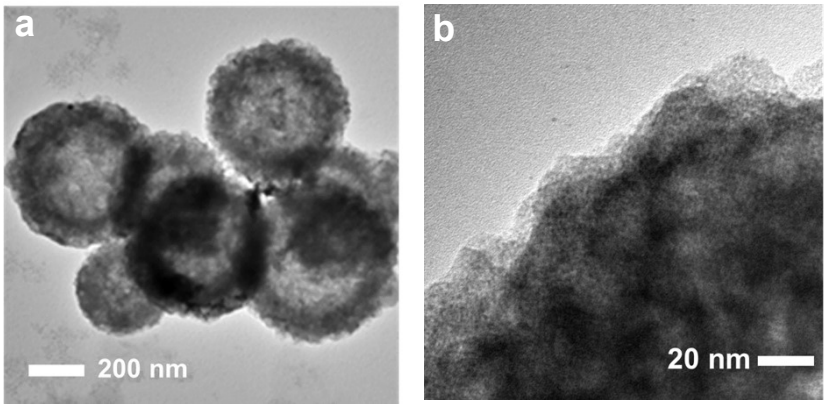

Fig. S9 TEM images of Ir/MoO_2-Mo_2C-800 after 700 hours of operation in an AEMWE at 200 mA cm^{-2}.

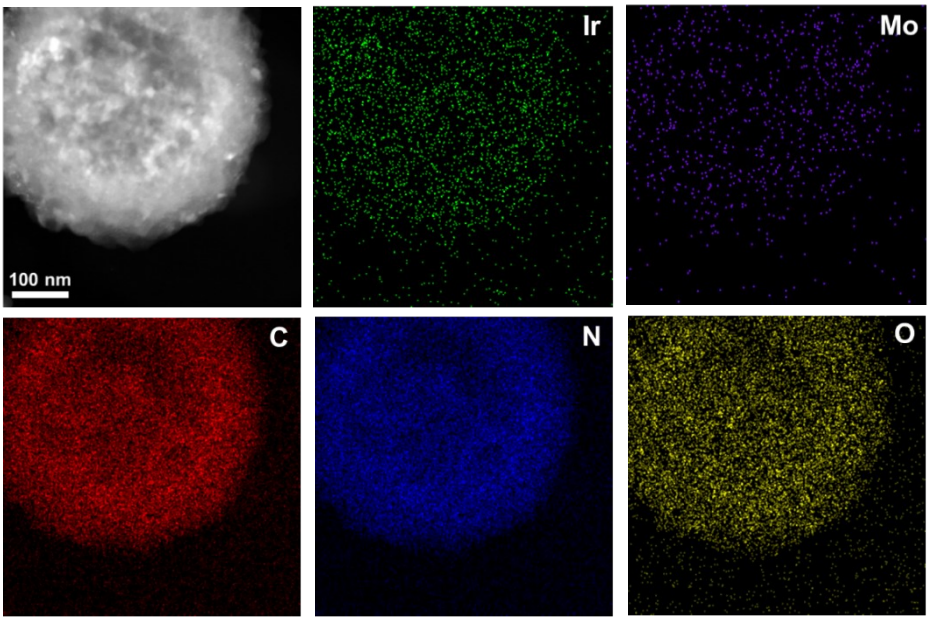

Fig. S10 Elemental distribution maps of Ir/MoO_2-Mo_2C-800 after 700 hours of operation in an AEMWE at 200 mA cm^{-2}.

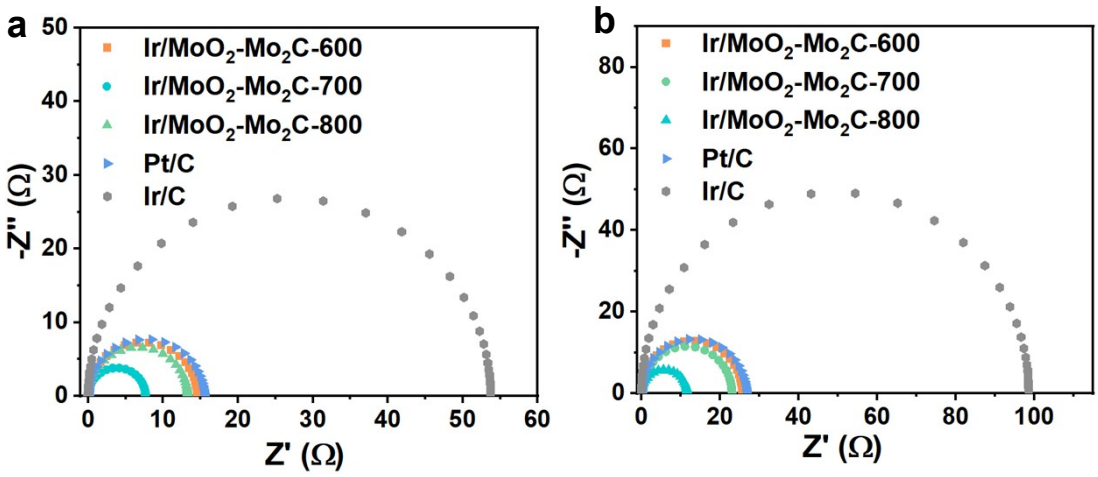

Fig. S11 Nyquist plots of Ir/MoO_2-Mo_2C-800 and other catalysts in (a) 0.5 M H_2SO_4 and (b) 1.0 M PBS solutions.

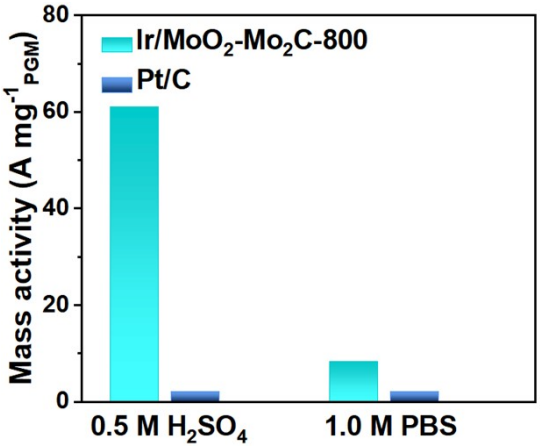

Fig. S12 The mass activities of Ir/MoO_2-Mo_2C-800 and Pt/C were measured at overpotentials of 100 mV (neutral) and 30 mV (acidic).

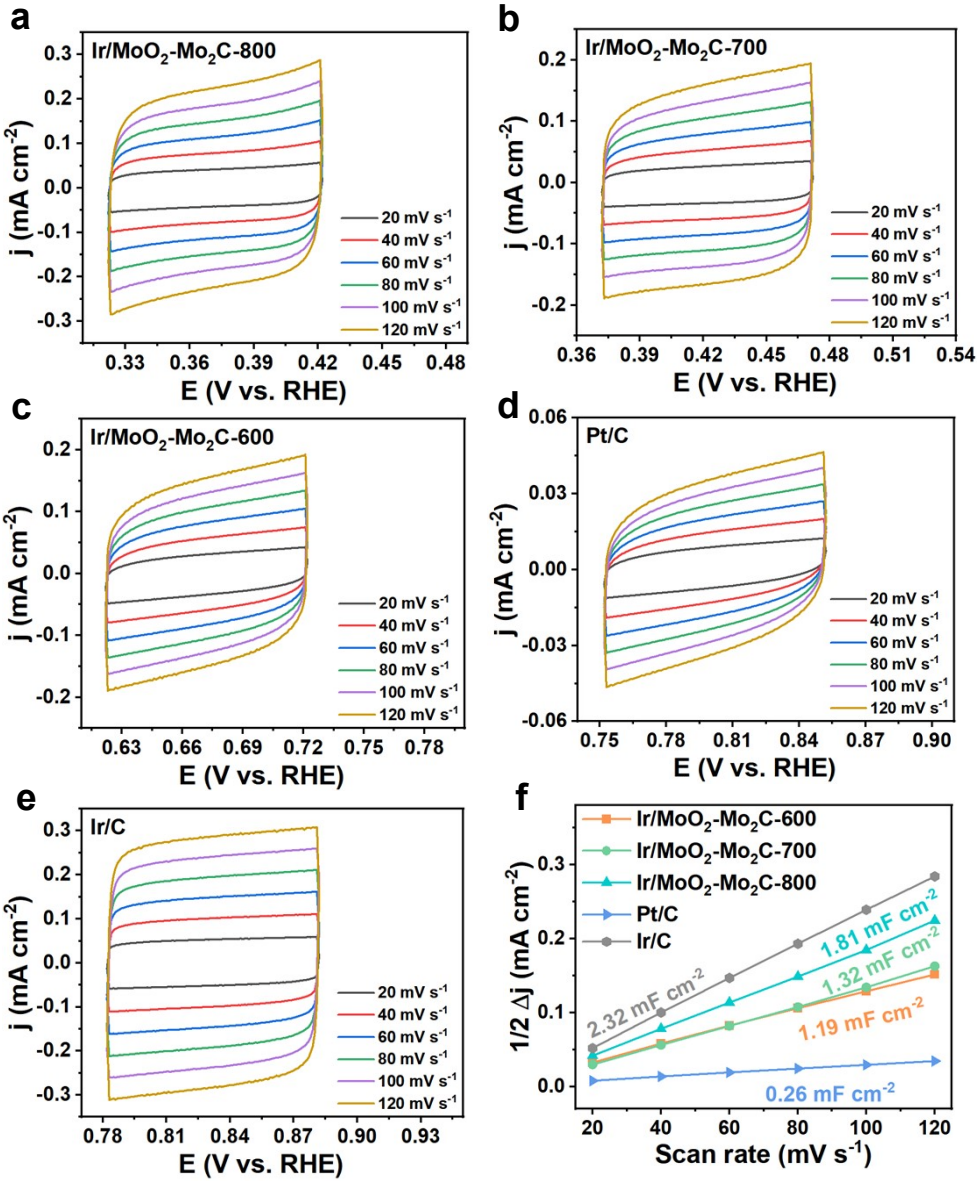

Fig. S13 CV curves with different scan rates from 20 to 120 mV s^{-1} in 0.5 M H_2SO_4 for (a) Ir/MoO_2-Mo_2C-800, (b)

Ir/MoO_2-Mo_2C-700, (c) Ir/MoO_2-Mo_2C-600, (d) Pt/C, and (e) Ir/C. (f) C_{dl} test of the as-synthesized samples.

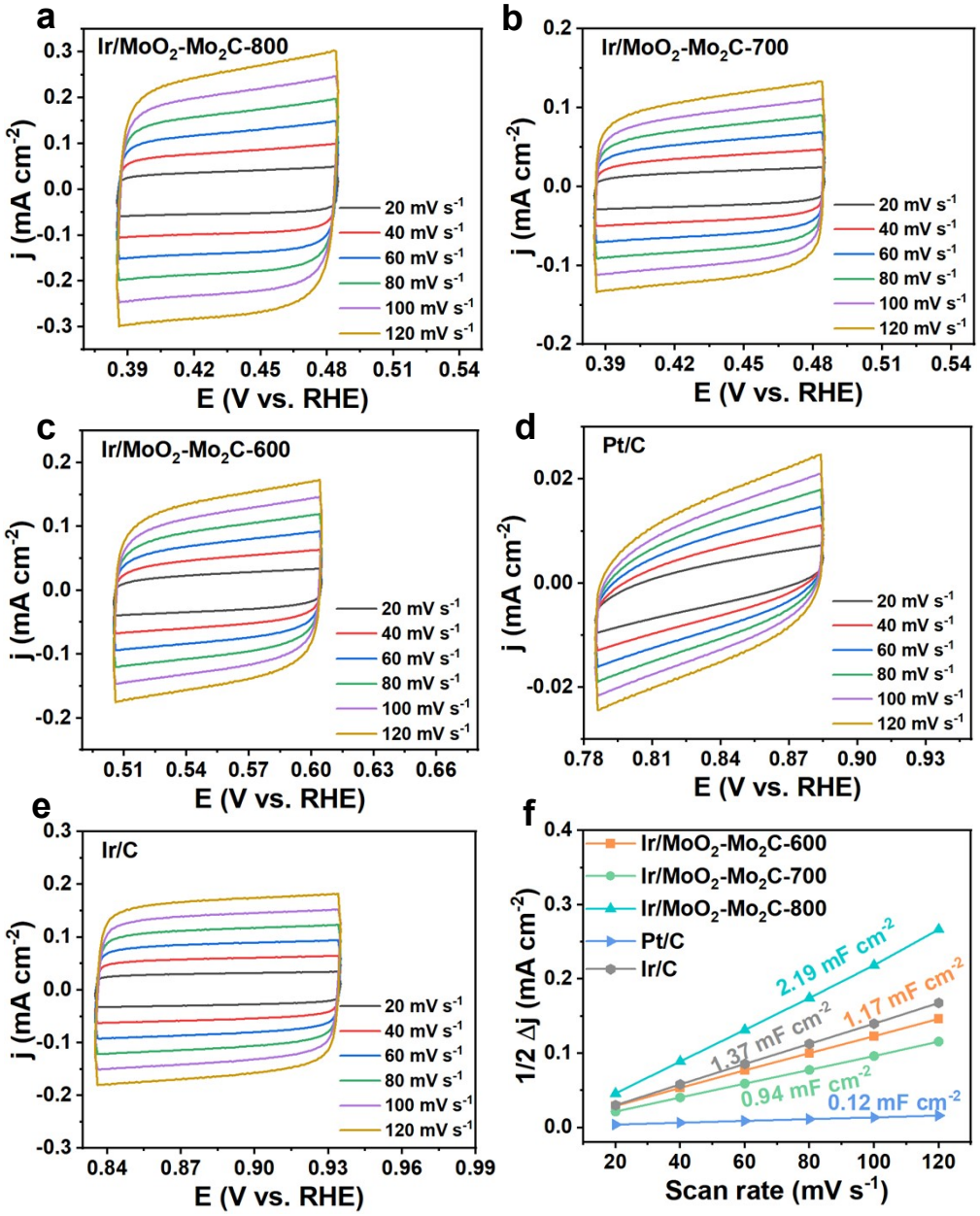

Fig. S14 CV curves with different scan rates from 20 to 120 mV s^{-1} in 1.0 M PBS for (a) Ir/MoO_2-Mo_2C-800, (b) Ir/MoO_2-Mo_2C-700, (c) Ir/MoO_2-Mo_2C-600, (d) Pt/C, and (e) Ir/C. (f) C_{dl} test of the as-synthesized samples.

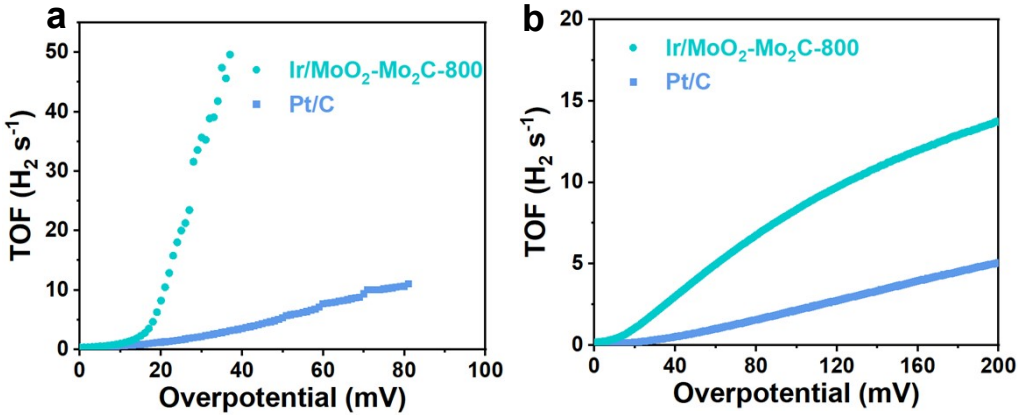

Fig. S15 TOF curves of Ir/MoO_2-Mo_2C-800 and other comparative samples in (a) 0.5 M H_2SO_4 solution and (b) 1.0 M PBS solutions.

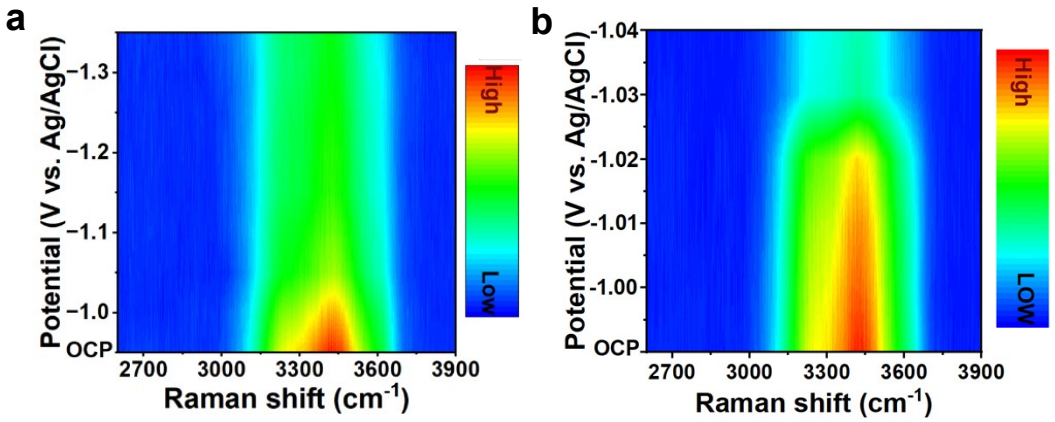

Fig. S16 Corresponding contour map of Ir/MoO_2-Mo_2C-800 in (a) 1.0 M KOH solution and (b) 0.5 M H_2SO_4 solutions.

Table S1. The ICP-OES results for different Ir/MoO_2-Mo_2C.

Catalysts	Ir loading (wt.%)
Ir/MoO_2-Mo_2C-800	14.92
Ir/MoO_2-Mo_2C-700	14.77
Ir/MoO_2-Mo_2C-600	14.62

Sample	Path	*CN*[a]	*R*(Å)[b]	σ^2 (Å^2)[c]	ΔE_0(Ev)[d]	*R* factor
Ir L_3-edge (S_0^2=0.744)						
Ir foil	Ir-Ir	12.0*	2.711±0.001	0.0032	8.9±0.5	0.0017
IrO_2	Ir-O	5.7±0.6	1.980±0.011	0.0027	9.6±1.3	0.0134
	Ir-O-Ir	3.5±1.0	3.104±0.035	0.0107	3.5±3.6	
	Ir-O-Ir	7.5±0.7	3.549±0.038			
Ir/MoO2-Mo2C-800	Ir-O	2.4±0.4	2.006±0.014	0.0047	9.4±1.8	0.0084
	Ir-Ir	6.7±1.0	2.711±0.007	0.0046		
	Ir-Mo	1.1±0.7	2.870±0.038	0.0048		

Table S2 The best-fitted EXAFS results of Ir foil, IrO_2, and Ir/MoO_2-Mo_2C-800.

[a]CN, coordination number; [b]R, the distance between absorber and backscatter atoms; [c]σ^2, the Debye Waller factor value; [d]ΔE_0, inner potential correction to account for the difference in the inner potential between the sample and the reference compound; R factor indicates the goodness of the fit. S_0^2 was fixed to 0.744, according to the experimental EXAFS fit of Ir foil by fixing *CN* as the known crystallographic value. * This value was fixed during EXAFS fitting, based on the known structure of Ir. Fitting conditions: *k* range：3.0-13.5; *R* range: 1.0-3.0; fitting space: R space; *k*-weight = 3. A reasonable range of EXAFS fitting parameters: $0.700 < S_0^2 < 1.000$; $CN > 0$; $\sigma^2 > 0$ Å^2; $|\Delta E_0| < 15$ eV; *R* factor < 0.02.

Table S3 Comparison of the HER performance for Ir/MoO_2-Mo_2C-800 catalyst with other electrocatalysts in alkaline solution

Catalysts	Overpotential at 10 mA cm^{-2} (mV)	Tafel Slope (mV dec^{-1})	References
Ir/MoO_2-Mo_2C-800	32	35.76	This work
IrCo/NC	33	53	[6]
Ir-Co/CF	49	36	[7]
IrCo@NC-500	45	80	[8]
IrNi-N-C	45	38	[9]
Ir_3Cu/C	111	99.4	[10]
Co@Ir/NC	121	73.8	[11]
Ir-NCNSs	125	107	[12]
Ir_{SA}-2NS-$Ti_3C_2T_x$	40.8	50.5	[13]
CoIr@CN	70	123.8	[14]
IrCo@NC	82	56	[15]

Table S4 Comparison of the HER performance for Ir/MoO_2-Mo_2C-800 catalyst with other electrocatalysts in acidic solution.

Catalysts	Overpotential at 10 mA cm^{-2} (mV)	Tafel Slope (mV dec^{-1})	References
Ir/MoO_2-Mo_2C-800	14	16.57	This work
Ir cluster@CoO/CeO_2	49	53	[16]
Co@Ir/NC-10%	29.4	41.9	[11]
Ir@N-G-750	19	26	[17]
IrCo/NC	32	36	[6]
Ir-Co-W NPs	35.82	38.4	[18]
IrFe/NC	41	22	[19]
CoIr@CN	25	24.1	[14]
Ir_3Cu/C	57	35	[10]
IrCo@NC-850	50	25	[15]
0.1Ni-NCNFs-5Ir	22	45.9	[20]

Table S5 Comparison of the HER performance for Ir/MoO_2-Mo_2C-800 catalyst with other electrocatalysts in neutral solution.

Catalysts	Overpotential at 10 mA cm^{-2} (mV)	Tafel Slope (mV dec^{-1})	References
Ir/MoO_2-Mo_2C-800	29	34.21	This work
Ir@NBD-C	37	81	[21]
IrPdH	60	160.30	[22]
Ir@Ni-NDC	31	46.9	[23]
Ir-NR/C	86	66.8	[24]
Ir/HfO_2@C	51	53	[25]
Ir_3-$Ni(OH)_2$/NF	43	67	[26]
IrP_2@NPC	90	87	[27]
DNP-IrNi	78	-	[28]
Li-$IrSe_2$	120	-	[29]
IrO_2-RuO_2/C	147	86	[30]

References

1. A. Salah, H. D. Ren, N. Al Ansi, F. Y. Yu, Z. L. Lang, H. Tan and Y. G. Li, *J. Mater. Chem. A*, 2021, **9**, 20518-20529.
2. S. I. Zabinsky, J. J. Rehr, A. Ankudinov, R. C. Albers and M. J. Eller, *Phys. Rev. B*, 1995, **52**, 2995-3009.
3. B. Ravel and M. Newville, *J. Synchrotron Rad.*, 2005, **12**, 537-541.
4. Y. Hao, S. F. Hung, W. J. Zeng, Y. Wang, C. Zhang, C. H. Kuo, L. Wang, S. Zhao, Y. Zhang, H. Y. Chen and S. Peng, *J. Am. Chem. Soc.*, 2023, **145**, 23659-23669.
5. H. Luo, L. Li, F. Lin, Q. Zhang, K. Wang, D. Wang, L. Gu, M. Luo, F. Lv and S. Guo, 2024, **36**, 2403674.
6. C. Wu, M. Zhang, F. Chen, H. Kang, S. Xu and S. Xu, *Dalton Trans.*, 2020, **49**, 13339-13344.
7. W. Wu, J. Liu and N. Johannes, *Int. J. Hydrogen Energy*, 2021, **46**, 609-621.
8. P. Jiang, J. Chen, C. Wang, K. Yang, S. Gong, S. Liu, Z. Lin, M. Li, G. Xia, Y. Yang, J. Su and Q. Chen, *Adv. Mater.*, 2018, **30**, 1705324.
9. D. Liu, Y. Zhao, C. Wu, W. Xu, S. Xi, M. Chen, L. Yang, Y. Zhou, Q. He, X. Li, B. Ge, L. Song, J. Jiang and Q. Yan, *Nano Energy*, 2022, **98**, 107296.
10. J. Yan, Y. Chang, J. Chen, M. Jia and J. Jia, *J. Colloid Interf. Sci.*, 2023, **642**, 779-788.
11. D. Li, Z. Zong, Z. Tang, Z. Liu, S. Chen, Y. Tian and X. Wang, *ACS Sustainable Chem. Eng.*, 2018, **6**, 5105-5114.
12. X. Wu, Z. Wang, K. Chen, Z. Li, B. Hu, L. Wang and M. Wu, *ACS Appl. Mater. Interfaces*, 2021, **13**, 22448-22456.
13. W. Lin, Y. R. Lu, W. Peng, M. Luo, T. S. Chan and Y. Tan, *J. Mater. Chem. A*, 2022, **10**, 9878-9885.
14. W. Chen, Y. Xie, X. Gao, L. Li and Z. Lin, *J. Mater. Chem. A*, 2022, **10**, 15543-15553.
15. Y. Q. Zhou, L. Zhang, H. L. Suo, W. Hua, S. Indris, Y. Lei, W. H. Lai, Y. X. Wang, Z. Hu, H. K. Liu, S. L. Chou and S. X. Dou, *Adv. Funct. Mater.*, 2021, **31**, 2101797.
16. L. Zhang, Y. Lei, Y. Yang, D. Wang, Y. Zhao, X. Xiang, H. Shang and B. Zhang, *Adv. Sci.*, 2024, **11**, 2407475.
17. X. Wu, B. Feng, W. Li, Y. Niu, Y. Yu, S. Lu, C. Zhong, P. Liu, Z. Tian, L. Chen, W. Hu and C. M. Li, *Nano Energy*, 2019, **62**, 117-126.
18. M. Kim, H. Kang, E. Hwang, Y. Park, W. Jeong, Y. J. Hwang and D.-H. Ha, *Appl. Surf. Sci.*, 2023, **612**, 155862.
19. P. Jiang, H. Huang, J. Diao, S. Gong, S. Chen, J. Lu, C. Wang, Z. Sun, G. Xia, K. Yang, Y. Yang, L. Wei and Q. Chen, *Appl. Catal., B*, 2019, **258**, 117965.
20. X. Chen, W. Gou, J. Xu, R. Qi, S. Ren, C. Wang, W. Chen, G. Yu and X. Lu, *Chem. Eng. J.*, 2023, **471**, 144481.
21. D. Xue, J. Cheng, P. Yuan, B. A. Lu, H. Xia, C. C. Yang, C. L. Dong, H. Zhang, F. Shi, S. C. Mu, J. S. Hu, S. G. Sun and J. N. Zhang, *Adv. Funct. Mater.*, 2022, **32**, 2113191.
22. D. Wang, X. Jiang, Z. Lin, X. Zeng, Y. Zhu, Y. Wang, M. Gong, Y. Tang and G. Fu, *Small*, 2022, **18**, 2204063.
23. J. Yang, Y. Shen, Y. Sun, J. Xian, Y. Long and G. Li, *Angew. Chem. Int. Edit.*, 2023, **62**, e202302220.
24. F. Luo, L. Guo, Y. Xie, J. Xu, K. Qu and Z. Yang, *Appl. Catal., B*, 2020, **279**, 119394.
25. W. Shao, Z. Xing, X. Xu, D. Ye, R. Yan, T. Ma, Y. Wang, Z. Zeng, B. Yin, C. Cheng and S. Li, *J. Am. Chem. Soc.*, 2024, **146**, 27486-27498.
26. Y. Tong, H. Mao, Q. Sun, P. Chen, F. Yan and J. Liu, *ChemCatChem*, 2020, **12**, 5720-5726.
27. W. L. Yu, J. Q. Chi and B. Dong, *J. Mater. Chem. A*, 2021, **9**, 2195-2204.
28. K. R. Yeo, K. S. Lee, H. Kim, J. Lee and S. K. Kim, *Energy Environ. Sci.*, 2022, **15**, 3449-3461.
29. T. Zheng, C. Shang, Z. He, X. Wang, C. Cao, H. Li, R. Si, B. Pan, S. Zhou and J. Zeng, *Angew. Chem. Int. Edit.*, 2019, **58**, 14764-14769.
30. R. Samanta, P. Panda, R. Mishra and S. Barman, *Energy Fuels*, 2022, **36**, 1015-1026.